

Magnetism of Kitaev spin-liquid candidate material RuBr₃

Yoshinori Imai,^{1,*} Kazuhiro Nawa,² Yasuhiro Shimizu,³ Wakana Yamada,¹ Hideyuki Fujihara,¹ Takuya Aoyama,¹ Ryotaro Takahashi,² Daisuke Okuyama,² Takamasa Ohashi,³ Masato Hagihala,⁴ Shuki Torii,⁴ Daisuke Morikawa,² Masami Terauchi,² Takayuki Kawamata,⁵ Masatsune Kato,⁵ Hirotsada Gotou,⁶ Masayuki Itoh,³ Taku J. Sato,² and Kenya Ohgushi¹

¹*Department of Physics, Graduate School of Science, Tohoku University, 6-3 Aramaki-Aoba, Aoba-ku, Sendai, Miyagi 980-8578, Japan*

²*Institute of Multidisciplinary Research for Advanced Materials, Tohoku University, Katahira, Sendai, 980-857, Japan*

³*Department of Physics, Nagoya University, Furo-cho, Chikusa-ku, Nagoya 464-8602, Japan*

⁴*Institute of Materials Structure Science, High Energy Accelerator Research Organization (KEK), 203-1 Tokai, Ibaraki, 319-1106, Japan*

⁵*Department of Applied Physics, Graduate School of Engineering, Tohoku University, Sendai 980-8579, Japan*

⁶*Institute for Solid State Physics, University of Tokyo, Kashiwa, Chiba 277-8581, Japan*

The ruthenium halide α -RuCl₃ is a promising candidate for a Kitaev spin liquid. However, the microscopic model describing α -RuCl₃ is still debated partly because of a lack of analogue materials for α -RuCl₃, which prevents tracking of electronic properties as functions of controlled interaction parameters. Here, we report a successful synthesis of RuBr₃. The material RuBr₃ possesses BiI₃-type structure (space group: $R\bar{3}$) where Ru³⁺ form an ideal honeycomb lattice. Although RuBr₃ has a negative Weiss temperature, it undergoes a zigzag antiferromagnetic transition at $T_N = 34$ K, as does α -RuCl₃. Our analyses indicate that the Kitaev and non-Kitaev interactions can be modified in ruthenium trihalides by changing the ligand sites, which provides a new platform for exploring Kitaev spin liquids.

A theoretical breakthrough [1] has brought compounds with honeycomb lattices into the spotlight as candidates for quantum spin liquids. Kitaev proposed a model where $S = 1/2$ spins placed on a honeycomb lattice are coupled with their three nearest-neighbor spins with bond-dependent ferromagnetic Ising interactions [1]. This model is exactly solvable, and the ground state is a quantum spin liquid. The material α -RuCl₃ is the most promising candidate for a Kitaev spin liquid and has been actively studied in recent years [2–4]. In α -RuCl₃, Ru³⁺ form a honeycomb lattice in two-dimensional layers through an edge-sharing network of RuCl₆ octahedra. The detailed crystal structure of α -RuCl₃ is debated [5–8]. Recent studies on high-quality single crystals report that it has an AlCl₃-type crystal structure at room temperature with a slightly distorted honeycomb lattice (space group: $C2/m$), and that below a structural transition temperature of 150 K, it has a BiI₃-type structure with an ideal honeycomb lattice (space group: $R\bar{3}$, Fig. 1(a)) [9–11]. Instead of the expected spin-liquid state owing to the frustrated nature of the Kitaev interaction K , α -RuCl₃ shows a zigzag antiferromagnetic order [6]. The antiferromagnetic transition temperature, $T_N = 7 - 14$ K, is very sensitive to the details of the crystal structure [7, 12]. The long-range antiferromagnetic order originates from the sizable contributions of non-Kitaev interactions such as the Heisenberg interaction J and off-diagonal interaction Γ . In fact, the extended model that takes such contributions into account (the J - K - Γ model) is useful for describing magnetic properties

of α -RuCl₃. The Hamiltonian is written as

$$\mathcal{H} = \sum_{\langle i,j \rangle \in NN} \left(JS_i \cdot S_j + KS_i^\gamma S_j^\gamma + \Gamma \left(S_i^\alpha S_j^\beta + S_i^\beta S_j^\alpha \right) \right), \quad (1)$$

where S_i^γ denotes the γ component of the spin-1/2 operator of site i (γ being the direction perpendicular to the edge-sharing plane) [13–15]. By assuming appropriate values of the parameters J , K , and Γ , this Hamiltonian (eq. 1) can well explain various magnetic behaviors of α -RuCl₃, including the zigzag antiferromagnetic order, the field-induced Kitaev spin-liquid state, and magnetic excitations in Raman and inelastic neutron spectra [13, 16–18]. Earlier works have revealed a dominant ferromagnetic Kitaev interaction of $K = -3 - -25$ meV and sizable contributions from the other terms, $|J/K| \sim 0.05 - 0.25$ and $|\Gamma/K| \sim 0.21 - 0.99$ [19]. Hence, α -RuCl₃ is still far from the ideal Kitaev limit, $|K| \gg |J|, |\Gamma|$. However, no methods to tune the parameters J , K , and Γ have been established experimentally, and no state closer to the Kitaev limit has been achieved yet. This is partly because there are no analogue materials for α -RuCl₃.

Here, we focus on two polymorphs of RuCl₃: an α one with a honeycomb structure and a β one with a one-dimensional chain structure (space group: $P6_3/mcm$) [20]. While both polymorphs exist for RuCl₃, only the chain structure is known for RuBr₃ [20, 21]. Because α -RuCl₃ is more densely packed than β -RuCl₃, one expects that RuBr₃ with the honeycomb structure can be obtained by keeping RuBr₃ with the chain structure under high pressure and high temperature. Actually, recent first-principles calculations predict the stability of RuBr₃

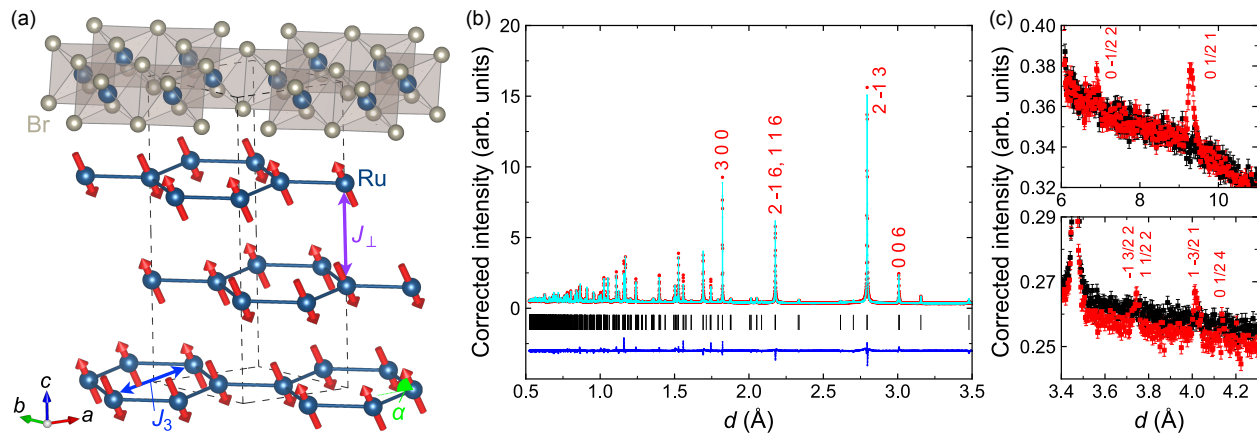


FIG. 1. Crystal and magnetic structures of RuBr_3 with the BiI_3 structure. (a) Schematic of crystal and magnetic structures refined from the neutron diffraction pattern. This figure is drawn using VESTA [41]. α is the angle of the magnetic moment from the honeycomb plane, and J_3 and J_\perp are the third-nearest-neighbor and the interlayer Heisenberg interactions, respectively. (b) Neutron diffraction pattern collected at 300 K by the backscattering (BS) bank. The red dots, cyan curve, and blue curve represent the observed intensities, calculated intensities, and difference between them. The difference is shifted for clarity. The vertical black bars indicate the peak position expected from the space group $R\bar{3}$. (c) Neutron diffraction patterns focused on the magnetic reflections. Intensities at 3 and 100 K are represented by the red and black dots, respectively. The upper and lower panels are data collected by the quarter-angle (QA) and low-angle (LA) detector banks, respectively.

with the honeycomb structure, which can be foiled into a monolayer limit [22]. Replacing Cl with Br is expected to have two effects: lattice expansion owing to the larger ionic radius of Br^- than that of Cl^- , and increased covalency of Ru-Cl/Br bonds owing to the up-floating of Br: $4p$ bands compared with Cl: $3p$ bands. As will be discussed later, both effects bring the system closer to the $|K| \gg |J|$, $|\Gamma|$ regime.

The X-ray diffraction pattern of RuBr_3 synthesized at high pressure is totally different from that of RuBr_3 with the chain structure (see Supplementary Fig. S1). To clarify the crystal structure, we measured the high-resolution neutron powder diffraction at various temperatures; the pattern collected at 300 K is shown in Fig. 1(b). Among several crystal structures with different stacking sequences of the transition-metal trihalides [23–26], the BiI_3 structure with the space group $R\bar{3}$ (Fig. 1(a)) best reproduces the experimental data. We cannot find any signatures of a structural transition such as peak splitting down to 3 K. The crystallographic data obtained through the Rietveld analysis are summarized in the supplementary information. In the refined structure, the Ru atoms in the unit cell are related to each other through the threefold rotation axis along the c -direction, and the network formed by the nearest-neighbor Ru–Ru bonds is a regular honeycomb lattice. This indicates that the newly developed RuBr_3 provides an ideal platform for exploring Kitaev spin liquids. Henceforth, we discuss the electronic properties of RuBr_3 with the $R\bar{3}$ structure.

Figure 2(a) shows the temperature dependence of the resistivity ρ for RuBr_3 . The data show a thermally acti-

vated temperature dependence, which is consistent with a strongly spin-orbital-coupled Mott insulator. The activation energy is $E_g \sim 0.21$ eV. Figure 2(b) shows the temperature dependence of the magnetic susceptibility χ under a magnetic field of $\mu_0 H = 1$ T. The data at 200–300 K well follow Curie-Weiss behavior, $\chi = C_{\text{CW}}/(T - \theta_{\text{CW}})$, with a Curie constant of $C_{\text{CW}} = 0.699$ emu/mol and a Weiss temperature of $\theta_{\text{CW}} = -58$ K. The effective moment per ruthenium ion, μ_{eff} , is calculated to be $2.36 \mu_B$ from the relation $C_{\text{CW}} = N_A \mu_{\text{eff}}^2 / 3k_B$, where N_A and k_B are the Avogadro constant and the Boltzmann constant, respectively. The negative Weiss temperature indicates the predominance of the antiferromagnetic correlation in this system. Turning to the low-temperature regime, χ shows a broad peak around $T^* = 60$ K, which is most likely related to the development of antiferromagnetic correlations. When the system is cooled further, χ shows a kink characterized by a sharp peak in $d\chi/dT$ at $T_N = 34$ K, as shown in Fig. 3(a). This kink anomaly corresponds to the formation of long-range antiferromagnetic order. This interpretation is supported by the result for the specific heat C , which shows a peak just around 34 K as shown in Fig. 3(b). The low-temperature part of C obeys a T^3 law ($C = \beta T^3$) as shown in the inset of Fig. 3(b), which can be explained by contributions from Debye phonons and antiferromagnetic spin waves in three dimensions. If we suppose that spin-wave contributions are negligible, we obtain a Debye temperature of $\theta_D = 159$ K from the formula $\beta = 12\pi^4 N R / 5\theta_D^3$, where N is the number of atoms per formula unit and R is the gas constant.

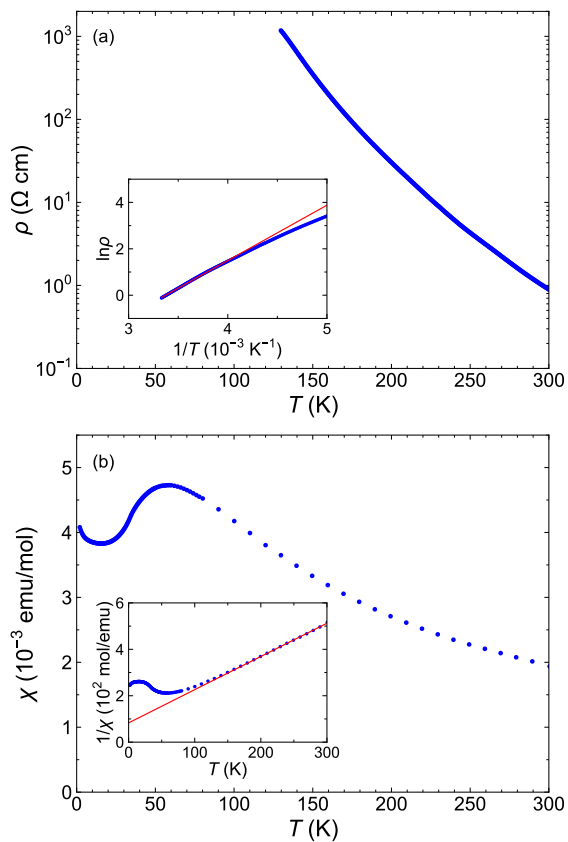


FIG. 2. Basic electronic properties of RuBr_3 with the BiI_3 structure. (a) Temperature (T) dependence of the resistivity (ρ). The inset shows the Arrhenius plot, and the fitting result is shown by the red line. (b) Temperature dependence of the magnetic susceptibility (χ) under a magnetic field of $\mu_0 H = 1$ T. The inset shows the inverse of χ . The data at 200 – 300 K are fitted with the Curie-Weiss law, and the fitting results are shown by the red line.

To investigate the spin dynamics, we performed nuclear quadrupole resonance (NQR) spectroscopy. Figures 4(a) and (b) show NQR spectra of ^{81}Br and ^{79}Br (nuclear spin $I = 3/2$) for RuBr_3 at 40–280 K. The resonance frequency scales well with the electric quadrupole moment ($^{81}Q = 0.276b$, $^{79}Q = 0.330b$, $b = 10^{-28} \text{ m}^2$). A single NQR spectrum for each nucleus is consistent with an $R\bar{3}$ structure that contains one Br site. The temperature dependence of the NQR frequency reflects an enhancement of the electric field gradient via thermal lattice contraction. Upon further cooling, the NQR spectrum splits below 34 K, clearly showing the emergence of a spontaneous local field due to the antiferromagnetic order. Figure 3(c) shows the temperature dependence of the ^{79}Br and ^{81}Br nuclear spin-lattice relaxation rate $1/T_1$. The values for both isotopes scale well with the square of the gyromagnetic ratio, as expected for predominant spin fluctuations. An increase in $1/T_1$ from about 60 K shows the growth of antiferromagnetic correlation; this is in harmony with the broad peak structure at T^* in χ .

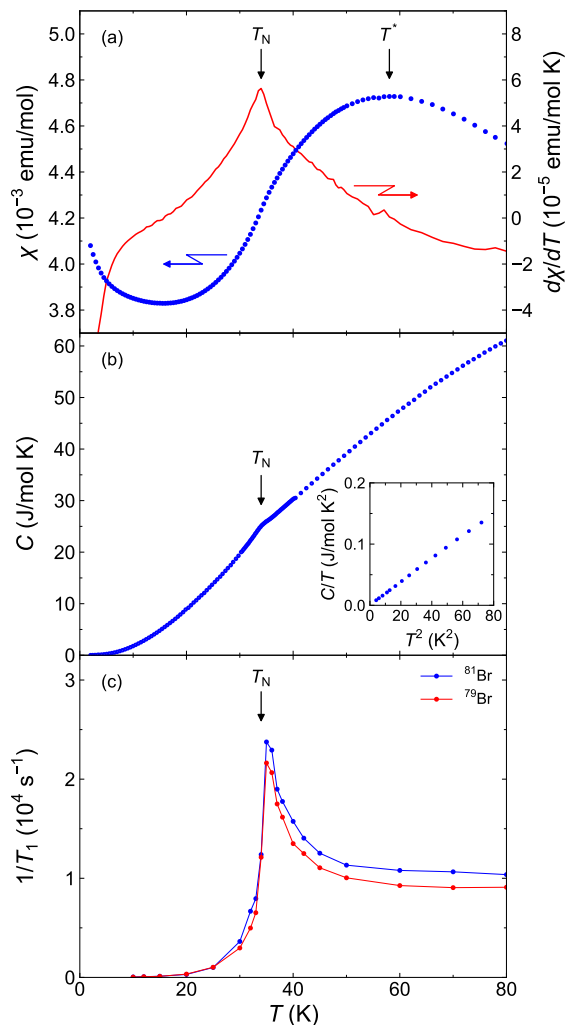


FIG. 3. Electronic properties near the antiferromagnetic transition for RuBr_3 with the BiI_3 structure. (a-c) Temperature (T) dependences of (a) the magnetic susceptibility (χ) and temperature differential of χ ($d\chi/dT$) under a magnetic field of $\mu_0 H = 1$ T, (b) the specific heat (C) under a zero magnetic field, and (c) the ^{79}Br and ^{81}Br nuclear spin-lattice relaxation rate $1/T_1$. In the inset of (b), C/T is plotted as a function of T^2 . The solid curves in (c) are guides for the eye.

The spin fluctuations divergently increase toward T_N , below which magnetic excitation is gapped, coinciding with the evolution of the order parameter as observed in the zero-field nuclear magnetic resonance (NMR) spectrum (Fig. 4(c)).

To reveal the magnetic structure, we performed neutron diffraction measurements at low temperature, and the collected patterns are shown in Fig. 1(c). At least five peaks are found at 3 K, while there are none at 100 K. These peaks can be indexed with the magnetic modulation vector $\mathbf{k} = (0, 1/2, 1)$. Initial candidates for determining the magnetic structure were obtained using magnetic representation theory [27]. The magnetic representations for the Ru moments were decom-

posed into two one-dimensional representations (IR1 and IR2) of the \mathbf{k} -group with the magnetic modulation vector $\mathbf{k} = (0, 1/2, 1)$ (see the supplementary information for the details of the IRs). The powder neutron diffraction pattern was well fit with the IR2 representation, which represents a zigzag antiferromagnetic structure (Fig. 1(a)). A zigzag order at low temperature in RuBr₃ agrees with the theoretical prediction, which takes electron correlation into account [22]. The magnetic moment is tilted, and its angle from the ab -plane is $\alpha = 64(12)^\circ$ (Fig. 1(a)). The magnitude of the magnetic moment is estimated to be $m = 0.74(12) \mu_B$.

We here compare the experimental results for two honeycomb-based materials, RuBr₃ and α -RuCl₃. The material RuBr₃ has the $R\bar{3}$ structure in the whole temperature range below room temperature, contrasting with the structural transition at 150 K from the $C2/m$ to the $R\bar{3}$ structure in α -RuCl₃ [9–11]. The metal-metal bond distance is $d_{\text{Ru-Ru}} = 3.6438(2) \text{ \AA}$ in RuBr₃, which

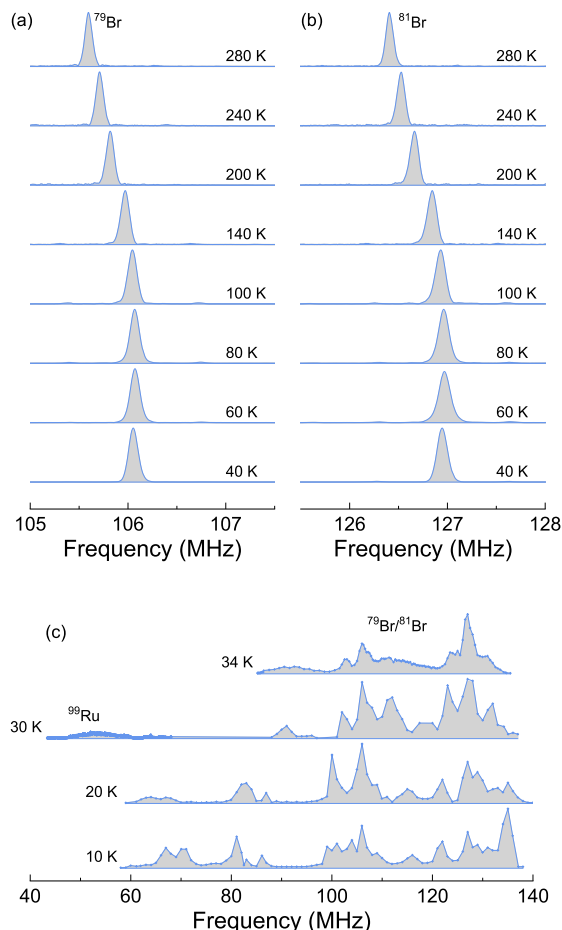


FIG. 4. Nuclear quadrupole resonance (NQR) spectra for RuBr₃ with the BiI₃ structure. (a, b) NQR spectra of (a) ⁷⁹Br and (b) ⁸¹Br above the antiferromagnetic transition temperature. (c) Zero-field Br and Ru nuclear magnetic resonance (NMR) spectra in the antiferromagnetically ordered state. A spectrum below 75 MHz comes from a ⁹⁹Ru NMR spectrum.

is much longer than the reported values $d_{\text{Ru-Ru}} = 3.43$ and 3.46 \AA in α -RuCl₃ [6, 7, 28]. The interlayer distance between the honeycomb planes is $d_{\perp} = 6.014(1) \text{ \AA}$ in RuBr₃, which is also longer than the reported $d_{\perp} = 5.72 \text{ \AA}$ in α -RuCl₃ [6, 7, 28]. These are the consequences of the larger ionic radius of Br⁻ than that of Cl⁻. The Ru-Cl/Br-Ru bond angle, which is an indicator of trigonal distortion, is closer to the ideal value of 90° for RuBr₃ ($\phi = 93.14(8)^\circ$) than for α -RuCl₃ ($\phi \sim 94^\circ$) [6, 7]. Hence, the $J_{eff} = 1/2$ state is still a good starting point in RuBr₃, which is also evidenced by the comparable effective magnetic moment: $\mu_{eff} = 2.36 \mu_B$ for RuBr₃ and $\mu_{eff} = 2.24 \mu_B$ for α -RuCl₃. The crucial difference between the two materials is the dominant magnetic interaction. In RuBr₃, there are fairly strong antiferromagnetic interactions characterized by a negative Weiss temperature of $\theta_{CW} = -58 \text{ K}$; in α -RuCl₃, there are ferromagnetic interactions characterized by a positive Weiss temperature of $\theta_{CW} = 19 \text{ K}$. Nevertheless, both compounds have zigzag magnetic order at low temperature. The magnetic order in RuBr₃ is more robust than in α -RuCl₃. This can be seen from the differences in T_N ($T_N = 34 \text{ K}$ for RuBr₃ and $T_N = 7-14 \text{ K}$ for α -RuCl₃) and the ordered magnetic moment ($m = 0.74(12) \mu_B$ for RuBr₃ and $m = 0.4-0.7 \mu_B$ for α -RuCl₃ [6–8, 10]). The tilt angle of the magnetic moment from the honeycomb plane is $\alpha = 64(12)^\circ$ in RuBr₃, which is larger than $\alpha = 32-35^\circ$ in α -RuCl₃ [7, 29]. Concerning magnetic fluctuations above T_N , both materials show an enhancement in $1/T_1$ toward T_N below nearly the same temperature, $\sim 60 \text{ K}$ [11]. However, the broad peak structure in the χ curve in this temperature regime is only seen in RuBr₃.

We now discuss the microscopic origin of the similarity/difference in magnetic properties of RuBr₃ and α -RuCl₃ on the basis of the $J-K-\Gamma$ model (eq. 1). The $J-K-\Gamma$ model contains the zigzag magnetic order as the ground state in a wide parameter space. Let us first discuss how the replacement of Cl with Br influences J , K , and Γ . The leading terms of J , K , and Γ deduced from perturbation theory can be written as follows [13, 30–33]:

$$J \simeq \frac{4 t_{dd}^2}{9 U}, \quad K \simeq -\frac{8 t_{dpd}^2 J_H}{3 U U}, \quad \Gamma \simeq -\frac{16 t_{dpd} t_{dd} J_H}{9 U U}, \quad (2)$$

where U and J_H are the Coulomb repulsion and the Hund coupling between t_{2g} electrons at the same site, respectively. These exchange interactions are sensitive to the direct hopping between nearest-neighbor t_{2g} orbitals, t_{dd} , and the indirect hopping between nearest-neighbor t_{2g} orbitals via ligand p orbitals, t_{dpd} . Replacing Cl with Br brings about drastic change especially in t_{dd} and t_{dpd} . Because $d_{\text{Ru-Ru}}$ for RuBr₃ is much longer than for α -RuCl₃, replacing Cl with Br results in a significant decrease in t_{dd} . The t_{dpd} values would be enhanced by replacing Cl with Br, because Br $4p$ orbitals are more strongly hybridized with Ru $4d$ orbitals than Cl $3p$ orbitals. As a

result, RuBr₃ is expected to have a higher $|K|$ and lower $|J/K|$ and $|\Gamma/K|$ than α -RuCl₃. Therefore, replacing Cl with Br drives the system closer to the Kitaev spin-liquid limit. This is clearly evidenced by the tilt angle of the magnetic moment from the honeycomb plane, α . Theoretical calculations based on the $J - K - \Gamma$ model indicate that α monotonically increases by approaching the Kitaev spin-liquid limit in the zigzag antiferromagnetic phase [14, 34–36]. Our experimental observation of larger α in RuBr₃ than in α -RuCl₃ is persuasive evidence that RuBr₃ is closer to the Kitaev spin-liquid limit than α -RuCl₃.

This then raises a new question of why the zigzag antiferromagnetic order in RuBr₃ is more stable than in α -RuCl₃, even though RuBr₃ is closer to the Kitaev spin-liquid limit with much geometrical frustration. One possible answer is that the energy scale of the $J - K - \Gamma$ model becomes much larger in RuBr₃ than in α -RuCl₃; however, this idea does not account for the difference in sign of the Weiss temperature between RuBr₃ and α -RuCl₃. The other plausible reason for the stable magnetic order in RuBr₃ is obtained by going beyond the $J - K - \Gamma$ model. The negative Weiss temperature in RuBr₃ implies a significant contribution from the antiferromagnetic non-Kitaev interactions. The possible candidates are the third-nearest-neighbor Heisenberg interaction $J_3 (> 0)$ and the interlayer coupling $J_\perp (> 0)$, which are shown in Fig. 1(a). These exchange interactions are believed to play an important role in the formation of zigzag antiferromagnetic order [13, 32, 37–39]. The hopping processes responsible for both J_3 and J_\perp occur through Ru4*d*–Br4*p*–Br4*p*–Ru4*d* paths [3, 39], which are pronounced owing to the enhanced hopping integrals between Ru4*d*–Br4*p* and Br4*p*–Br4*p* orbitals. Let us estimate the energy scale of J_3 and J_\perp . In the mean-field approximation, the Weiss temperature for a powder-averaged system is [39, 40]

$$k_B \theta_{\text{CW}} = -\frac{3}{4} \left(J + \frac{1}{3}K + J_3 + \frac{1}{3}J_\perp \right). \quad (3)$$

If we suppose that J is negligible, we can conclude from the negative Weiss temperature that $|3J_3 + J_\perp|$ is at least comparable to K . Our argument based on angle α in the preceding paragraph is not altered considerably, because it is not sensitive to the third-nearest-neighbor Heisenberg interaction [35, 36]. Validation of our approach requires experimental studies using RuBr₃ single crystals and support from theoretical studies.

In conclusion, we successfully synthesized RuBr₃ with a BiI₃-type structure (space group: $R\bar{3}$), where Ru³⁺ form an ideal honeycomb lattice. RuBr₃ shows a zigzag antiferromagnetic transition at $T_N = 34$ K, which is significantly higher than $T_N = 7 - 14$ K in α -RuCl₃. Our results indicate that the Kitaev and non-Kitaev interactions can be modified in ruthenium trihalides by changing the ligand sites, and provide a new platform

for exploring Kitaev spin liquids.

Methods

The RuBr₃ polycrystalline sample with the BiI₃ structure (space group: $R\bar{3}$) was synthesized using a cubic-anvil high-pressure apparatus. The starting material, commercially available RuBr₃ with the chain structure (space group: $P6_3/mcm$), was placed in a gold or platinum capsule and loaded into a pyrophyllite cube. These were pressurized at ~ 4 GPa and heated at $\sim 400^\circ\text{C}$ for 30 minutes. The electrical resistivity was measured using the four-terminal method over the temperature range 2 – 300 K. Magnetic susceptibility measurements were performed using a superconducting quantum interference device (SQUID) magnetometer. The specific heat was measured using the thermal-relaxation method at temperatures as low as 2 K under a magnetic field of $\mu_0 H = 0 - 9$ T using a commercial apparatus (Physical Property Measurement System, Quantum Design).

Powder neutron diffraction experiments were performed using the high-resolution time-of-flight (TOF) neutron powder diffractometer SuperHRPD installed at the beam line BL08 of J-PARC [42]. A powder sample of ~ 1.4 g was loaded into a vanadium-nickel cylindrical sample can with a diameter of 6 mm. The sample can was then put in a ⁴He closed-cycle refrigerator with the lowest attainable temperature of 3 K. SuperHRPD has three sets of detector banks: backscattering (BS), quarter-angle (QA), and low-angle (LA). The LA detector bank, which is in the low Q range, has the advantage of detecting magnetic reflections, while the BS detector bank, which achieves high resolution, is useful for investigating crystal structure precisely. The observed intensities were corrected for neutron absorption numerically. Rietveld analyses were done using the Fullprof software suite [43].

All three diffraction patterns were simultaneously used with the same weighting in the crystal-structure refinement, while the diffraction patterns from the QA and LA detector banks with a d -range larger than 2.9 Å were used for the magnetic-structure refinement. A pseudo-Voigt function convoluted with back-to-back exponentials [44] was used to fit the peak profile. In addition, a phenomenological model of the anisotropic peak broadening induced by the strain was applied to the peak width [45], because the peak width cannot be described as a smooth function of the d -spacing. The Ru⁺ form factor was used for the magnetic structure refinement because the Ru³⁺ form factor was not available.

Nuclear quadrupole resonance (NQR) of ⁷⁹Br and ⁸¹Br was measured for 40–290 K. The NQR spectra were measured with the spin-echo method with the pulse interval $\tau = 15 - 20$ μs and $\pi/2$ duration = 1.5 – 2 μs . The NQR frequencies and intensities for ⁷⁹Br and ⁸¹Br were consistent with their nuclear spins (⁷⁹, ⁸¹ $I = 3/2$), electric quadrupole moments (⁷⁹ $Q = 0.33b$, ⁸¹ $Q = 0.28b$), and

natural abundances ($^{79}\text{W} = 50\%$, $^{81}\text{W} = 50\%$). At zero field, the nuclear spin-lattice relaxation rate $1/T_1$ was measured with the saturation recovery and evaluated by fitting the recovery curve into a single exponential function.

* imai@tohoku.ac.jp

- [1] Kitaev, A. Anyons in an exactly solved model and beyond. *Ann. Phys.* **321**, 2 – 111 (2006).
- [2] Jackeli, G. & Khaliullin, G. Mott insulators in the strong spin-orbit coupling limit: From Heisenberg to a quantum compass and Kitaev models. *Phys. Rev. Lett.* **102**, 017205 (2009).
- [3] Winter, S. M. *et al.* Models and materials for generalized Kitaev magnetism. *J. Phys.: Cond. Matt.* **29**, 493002 (2017).
- [4] Motome, Y. & Nasu, J. Hunting Majorana fermions in Kitaev magnets. *J. Phys. Soc. Jpn.* **89**, 012002 (2020).
- [5] Stroganov, E. V. & Ovchinnikov, K. V. Crystal structure of ruthenium trichloride. *Vestn. Leningr. Univ. Ser. 4* **14**, 151–152 (1968).
- [6] Johnson, R. D. *et al.* Monoclinic crystal structure of α - RuCl_3 and the zigzag antiferromagnetic ground state. *Phys. Rev. B* **92**, 235119 (2015).
- [7] Cao, H. B. *et al.* Low-temperature crystal and magnetic structure of α - RuCl_3 . *Phys. Rev. B* **93**, 134423 (2016).
- [8] Banerjee, A. *et al.* Proximate Kitaev quantum spin liquid behaviour in a honeycomb magnet. *Nat. Mater.* **15**, 733–740 (2016).
- [9] Kubota, Y., Tanaka, H., Ono, T., Narumi, Y. & Kindo, K. Successive magnetic phase transitions in α - RuCl_3 : XY-like frustrated magnet on the honeycomb lattice. *Phys. Rev. B* **91**, 094422 (2015).
- [10] Park, S. Y. *et al.* Emergence of the isotropic Kitaev honeycomb lattice with two-dimensional ising universality in α - RuCl_3 . Preprint at <https://arxiv.org/abs/1609.05690> (2016).
- [11] Nagai, Y. *et al.* Two-step gap opening across the quantum critical point in the Kitaev honeycomb magnet α - RuCl_3 . *Phys. Rev. B* **101**, 020414 (2020).
- [12] Sears, J. A. *et al.* Magnetic order in α - RuCl_3 : A honeycomb-lattice quantum magnet with strong spin-orbit coupling. *Phys. Rev. B* **91**, 144420 (2015).
- [13] Rau, J. G., Lee, E. K.-H. & Kee, H.-Y. Generic spin model for the honeycomb iridates beyond the Kitaev limit. *Phys. Rev. Lett.* **112**, 077204 (2014).
- [14] Chaloupka, J. & Khaliullin, G. Hidden symmetries of the extended Kitaev-Heisenberg model: Implications for the honeycomb-lattice iridates $A_2\text{IrO}_3$. *Phys. Rev. B* **92**, 024413 (2015).
- [15] Janssen, L., Andrade, E. C. & Vojta, M. Magnetization processes of zigzag states on the honeycomb lattice: Identifying spin models for α - RuCl_3 and Na_2IrO_3 . *Phys. Rev. B* **96**, 064430 (2017).
- [16] Sandilands, L. J., Tian, Y., Plumb, K. W., Kim, Y.-J. & Burch, K. S. Scattering continuum and possible fractionalized excitations in α - RuCl_3 . *Phys. Rev. Lett.* **114**, 147201 (2015).
- [17] Nasu, J., Knolle, J., Kovrizhin, D. L., Motome, Y. & Moessner, R. Fermionic response from fractionalization in an insulating two-dimensional magnet. *Nat. Phys.* **12**, 912–915 (2016).
- [18] Kasahara, Y. *et al.* Majorana quantization and half-integer thermal quantum Hall effect in a Kitaev spin liquid. *Nature* **559**, 227–231 (2018).
- [19] Laurell, P. & Okamoto, S. Dynamical and thermal magnetic properties of the Kitaev spin liquid candidate α - RuCl_3 . *Npj Quantum Mater.* **5**, 2 (2020).
- [20] Hillebrecht, H., Ludwig, T. & Thiele, G. About trihalides with TlI_3 chain structure: Proof of pair forming of cations in β - RuCl_3 and RuBr_3 by temperature dependent single crystal x-ray analyses. *Z. Anorg. Allg. Chem.* **630**, 2199–2204 (2004).
- [21] von Schnering, H. G., Brodersen, K., Moers, F., Breitenbach, H. K. & Thiele, G. Strukturuntersuchungen an β - RuCl_3 , RuBr_3 und RuJ_3 . *J. Less Common Met.* **11**, 288 – 289 (1966).
- [22] Ersan, F. *et al.* Exploring the electronic and magnetic properties of new metal halides from bulk to two-dimensional monolayer: RuX_3 ($X = \text{Br}, \text{I}$). *J. Magn. Magn. Mater.* **476**, 111–119 (2019).
- [23] Müller, U. *Inorganic Structural Chemistry, 2nd Edition* (Wiley, 2006).
- [24] Müller, U. & Conradi, E. Fehlordnung bei Verbindungen MX_3 mit schichtenstruktur i. berechnung des intensitätsverlaufs auf den streifen der diffusen röntgenstreuung. *Z. Kristallogr. Cryst. Mater.* **176**, 233 – 261 (1986).
- [25] Hillebrecht, H. *et al.* Structural and scanning microscopy studies of layered compounds MCl_3 ($M = \text{Mo}, \text{Ru}, \text{Cr}$) and MOCl_2 ($M = \text{V}, \text{Nb}, \text{Mo}, \text{Ru}, \text{Os}$). *J. Alloys Compd.* **246**, 70 – 79 (1997).
- [26] McGuire, M. A. Crystal and magnetic structures in layered, transition metal dihalides and trihalides. *Crystals* **7**, 121 (2017).
- [27] Izyumov, Y. & Naish, V. Symmetry analysis in neutron diffraction studies of magnetic structures: 1. a phase transition concept to describe magnetic structures in crystals. *J. Magn. Magn. Mater* **12**, 239 – 248 (1979).
- [28] Imai, Y., Konno, K., Hasegawa, Y., Aoyama, T. & Ohgushi, K. Hydrated lithium intercalation into the Kitaev spin liquid candidate material α - RuCl_3 . *Phys. Rev. B* **99**, 245141 (2019).
- [29] Sears, J. A. *et al.* Ferromagnetic Kitaev interaction and the origin of large magnetic anisotropy in α - RuCl_3 . *Nat. Phys.* **16**, 837–840 (2020).
- [30] Matsuura, H. & Ogata, M. A poor man’s derivation of quantum compass-Heisenberg interaction: Superexchange interaction in J-J coupling scheme. *J. Phys. Soc. Jpn.* **83**, 093701 (2014).
- [31] Nasu, J. & Motome, Y. Spin-orbit coupling in octamers in the spinel sulfide CuIr_2S_4 : Competition between spin-singlet and quadrupolar states and its relevance to remnant paramagnetism. *Phys. Rev. B* **90**, 045102 (2014).
- [32] Winter, S. M., Li, Y., Jeschke, H. O. & Valentí, R. Challenges in design of Kitaev materials: Magnetic interactions from competing energy scales. *Phys. Rev. B* **93**, 214431 (2016).
- [33] Motome, Y., Sano, R., Jang, S., Sugita, Y. & Kato, Y. Materials design of Kitaev spin liquids beyond the Jackeli–Khaliullin mechanism. *J. Phys.: Condens. Matter* **32**, 404001 (2020).
- [34] Kim, H.-S. & Kee, H.-Y. Crystal structure and magnetism in α - RuCl_3 : An ab initio study. *Phys. Rev. B*

- 93**, 155143 (2016).
- [35] Chaloupka, J. c. v. & Khaliullin, G. Magnetic anisotropy in the Kitaev model systems Na_2IrO_3 and RuCl_3 . *Phys. Rev. B* **94**, 064435 (2016).
- [36] Rusnačko, J., Gotfryd, D. & Chaloupka, J. c. v. Kitaev-like honeycomb magnets: Global phase behavior and emergent effective models. *Phys. Rev. B* **99**, 064425 (2019).
- [37] Katukuri, V. M. *et al.* Kitaev interactions between $j=1/2$ moments in honeycomb Na_2IrO_3 are large and ferromagnetic: insights from ab initio quantum chemistry calculations. *New J. Phys.* **16**, 013056 (2014).
- [38] Yamaji, Y., Nomura, Y., Kurita, M., Arita, R. & Imada, M. First-principles study of the honeycomb-lattice iridates Na_2IrO_3 in the presence of strong spin-orbit interaction and electron correlations. *Phys. Rev. Lett.* **113**, 107201 (2014).
- [39] Janssen, L., Koch, S. & Vojta, M. Magnon dispersion and dynamic spin response in three-dimensional spin models for $\alpha\text{-RuCl}_3$. *Phys. Rev. B* **101**, 174444 (2020).
- [40] Li, Y., Winter, S. M., Kaib, D. A. S., Riedl, K. & Valentí, R. Modified Curie-Weiss law for j_{eff} magnets. *Phys. Rev. B* **103**, L220408 (2021).
- [41] Momma, K. & Izumi, F. *VESTA3* for three-dimensional visualization of crystal, volumetric and morphology data. *J. Appl. Cryst.* **44**, 1272–1276 (2011).
- [42] Torii, S. *et al.* Super high resolution powder diffractometer at J-PARC. *J. Phys. Soc. Jpn.* **80**, SB020 (2011).
- [43] Rodríguez-Carvajal, J. Recent advances in magnetic structure determination by neutron powder diffraction. *Physica B: Condensed Matter* **192**, 55 – 69 (1993).
- [44] Von Dreele, R. B., Jorgensen, J. D. & Windsor, C. G. Rietveld refinement with spallation neutron powder diffraction data. *J. Appl. Cryst.* **15**, 581–589 (1982).
- [45] Stephens, P. W. Phenomenological model of anisotropic peak broadening in powder diffraction. *J. Appl. Cryst.* **32**, 281–289 (1999).

Acknowledgements

We would like to thank Yohei Yamaji, Takahiro Misawa, Hakuto Suzuki, Joji Nasu, and Yukitoshi Motome for fruitful discussions, and Takumi Hiraoka and Takeshi Yajima for their help in the X-ray diffraction measurements. This work was carried out under the Visiting Researcher's Program of the Institute for Solid State Physics, the University of Tokyo.

This work was financially supported by JSPS KAKENHI under Grant Numbers JP18H01159, JP18K03531, JP19H01837, JP19H04685, JP19H05822, JP19H05823, JP19H05824, JP19K21837, and JP20H01850; by the Murata Science Foundation; and by JST CREST under Grant Number JP19198318.